Published in final edited form as:

Science. 2019 February 08; 363(6427): 649–654. doi:10.1126/science.aat9120.

Innate immune recognition of glycans targets HIV nanoparticle immunogens to germinal centers

Talar Tokatlian[1,†], **Benjamin J. Read**[1,2,†], **Christopher A. Jones**[1], **Daniel W. Kulp**[3,4,5], **Sergey Menis**[4,5], **Jason Y.H. Chang**[1], **Jon M. Steichen**[4,5], **Sudha Kumari**[1], **Joel D. Allen**[6], **Eric L. Dane**[1], **Alessia Liguori**[5,7], **Maya Sangesland**[8], **Daniel Lingwood**[8], **Max Crispin**[4,5,6,7], **William R. Schief**[4,5,7,8,*], and **Darrell J. Irvine**[1,5,8,9,10,11,*]

[1]Koch Institute for Integrative Cancer Research, Massachusetts Institute of Technology, Cambridge, MA 02139 USA.

[2]Health Sciences and Technology, Harvard University and Massachusetts Institute of Technology, Cambridge, MA 02139 USA.

[3]Vaccine and Immunotherapy Center, The Wistar Institute, Philadelphia, PA 19104.

[4]International AIDS Vaccine Initiative Neutralizing Antibody Center, The Scripps Research Institute, La Jolla, CA 92037 USA.

[5]Center for HIV/AIDS Vaccine Immunology and Immunogen Discovery, The Scripps Research Institute, La Jolla, CA 92037 USA.

[6]Biological Sciences and the Institute for Life Sciences, University of Southampton, Southampton SO17 1BJ, UK.

[7]Immunology and Microbial Science, The Scripps Research Institute, La Jolla, CA 92037 USA.

[8]The Ragon Institute of Massachusetts General Hospital, Massachusetts Institute of Technology and Harvard University, Cambridge, MA 02139 USA.

[9]Department of Biological Engineering, Massachusetts Institute of Technology, Cambridge, MA 02139 USA.

[10]Department of Materials Science and Engineering, Massachusetts Institute of Technology, Cambridge, MA 02139 USA.

[11]Howard Hughes Medical Institute, Chevy Chase, MD 20815 USA.

Abstract

[*]Correspondence to: djirvine@mit.edu (D.J.I.); schief@scripps.edu (W.R.S.).

Authors Contributions: T.T. and B.J.R. designed and performed experiments, analyzed the data, and wrote the manuscript; C.A.J. performed experiments and analyzed data; D.W.K. designed and provided HIV immunogens and edited the manuscript; S.M. synthesized HIV immunogens for experiments; J.M.S. designed and provided HIV immunogens; S.K. developed lymph node processing and imaging protocols; J.Y.H.C. processed and imaged lymph node slices; E.L.D. carried out trimannose conjugation studies; A.L. developed and performed ELISA protocols; J.D.A. and M.C. carried out glycan analysis of the immunogens; M.S. and D.L. designed and synthesized influenza immunogens; W.R.S. provided expert advice and edited the manuscript; D.J.I. supervised the research and wrote the manuscript.

[†]These authors contributed equally to this work.

Competing interests: Authors declare no competing interests.

Data and materials availability: All data is available in the main text or the supplementary materials.

Arraying antigens in a multivalent nanoparticle form is often employed in vaccine design, but *in vivo* mechanisms underlying the enhanced immunity elicited by such vaccines remain poorly understood. Here we studied the fate of two different heavily glycosylated HIV antigens in protein nanoparticle or “free” forms following primary immunization. Unlike monomeric antigens, nanoparticles were rapidly shuttled to the follicular dendritic cell (FDC) network followed by concentration in germinal centers, in a complement-, mannose-binding lectin (MBL)-, and immunogen glycan-dependent manner. Loss of FDC localization in MBL-deficient mice or via immunogen deglycosylation significantly impacted antibody responses. These findings identify a novel innate immune-mediated recognition pathway promoting humoral immunity to particulate antigens, with broad implications for humoral immunity to microbes and the design of improved vaccines.

One Sentence Summary:

Recognition of densely-arrayed glycans by mannose-binding lectin triggers trafficking of nanoparticle immunogens to B cell follicles.

Viruses and bacteria are nano- to micron-sized particles, and the immune system has thus evolved to recognize and respond to particulate antigens. Nanoparticles are efficiently trafficked to lymphoid tissues through afferent lymph, are effectively internalized and processed for antigen presentation by dendritic cells, and potently activate B cells via crosslinking of B cell receptors (BCRs) (1). These features of immune recognition have motivated the use of nanoparticulate antigens in licensed vaccines such as the human papilloma virus and hepatitis B vaccines (2, 3), and have motivated the design of nanoparticle forms of immunogens in the development of new vaccines (4–6). For example, evidence from preclinical animal models indicates that compared to monomeric antigens, nanoparticulate HIV immunogens more effectively activate low-affinity germline precursor B cells (6–9), promote enhanced follicular helper T cell (T_{fh}) induction and germinal center (GC) responses (9, 10), and enhance the induction of neutralizing antibody responses (9, 11, 12). However, the mechanisms by which these many events in adaptive immunity are influenced by the physical form of immunogens remain poorly understood.

To define pathways regulating the immune response to multivalent particulate antigens *in vivo*, we examined the fate of two distinct HIV envelope antigens as soluble “monomers” or as protein nanoparticles: a germline-targeting gp120 immunogen, engineered outer domain-GT8 (eOD) (6, 13–15); and a gp140 trimer. The envelope trimer, MD39, is an improved version of BG505 SOSIP gp140 with enhanced thermal stability and expression level and reduced exposure of the V3 loop (8, 16). eOD was formulated as a ~32 nm diameter nanoparticle, eOD-GT8 60mer, (eOD-60mer) by fusion to a bacterial protein lumazine synthase, which self-assembles into a 60-mer as previously described (Fig. 1A) (13–15). A ~40 nm diameter nanoparticle form of MD39 (MD39–8mer) was generated by fusing the MD39 gp140 chain to an archaeal ferritin; 24 subunits of ferritin self-assemble to form a nanoparticle (ferritin core outer diameter ~12 nm) displaying 8 copies of gp140 trimer (Fig. 1B) (12, 17). MD39–8mer eluted as a relatively uniform peak in size exclusion chromatography, showed an ELISA binding profile to neutralizing and non-neutralizing monoclonal antibodies consistent with expectations for the MD39 trimer (12), and was

observed to have a reasonably homogeneous morphology by TEM (Fig. 1B, fig. S1A–C). *In vitro,* both eOD-60mer and MD39–8mer stimulated stronger calcium signaling in VRC01-expressing B cells than their monomer counterparts (ref. (6) and fig. S1D). Mice immunized with the nanoparticle forms of eOD and MD39 elicited higher IgG titers (up to 90-fold greater) compared to the soluble immunogens (Fig. 1C–E). Analysis of responding cells in lymph nodes revealed that Tfh responses were not altered by nanoparticle immunization (Fig. 1F–G), but GC B cells were significantly increased (Fig. 1H–I). A deeper analysis of eOD-immunized animals further showed that polyclonal IgGs isolated from eOD-60mer-immunized sera exhibited lower off-rates than IgG from monomer-immunized animals, indicative of enhanced affinity maturation (Fig. 1J, fig. S2A–B). Thus, the nanoparticle forms of both eOD gp120 and trimer elicited substantially enhanced humoral responses *in vivo*.

To understand these stark differences in immunogenicity, we examined the lymphatic trafficking and tissue localization of each immunogen. Whole-tissue fluorescence measurements of infra-red dye-labeled immunogens in draining lymph nodes (dLNs) showed higher total accumulation of both nanoparticle formulations in dLNs at 3 days post immunization compared to monomeric forms (Fig. 2A). However, confocal imaging of cleared whole dLNs revealed that soluble MD39 accumulated primarily in the subcapsular sinus and medullary areas, while MD39–8mer was observed to begin concentrating within follicles by day 3 and was strongly co-localized with FDCs by day 7 (Fig. 2B–C). Liposomes (~95 nm diam.) surface-conjugated with densely packed MD39 also exhibited FDC accumulation over 7 days post immunization, though with a lower efficiency than the smaller ferritin-based nanoparticles, suggesting FDC targeting is independent of the nature of the nanoparticle core (Fig. 2C, fig. S3A) (8). Trafficking of eOD monomer vs. 60-mer was even more distinct: While eOD monomer showed low levels of accumulation in dLNs over a 14 day timecourse and primarily colocalized with SIGN-R1^{+} macrophages as reported previously for other gp120 antigens (18), eOD-60mer was already beginning to co-localize with FDCs after 24 hours (Fig. 2D, fig. S3B–C). By day 7 eOD nanoparticles were almost exclusively localized within the FDC network and persisted there for ~4 weeks (Fig. 2D–E, fig. S3D–E); FDC localization occurred in the presence or absence of co-administered adjuvant, albeit with lower overall accumulation (fig. S3F). FDC targeting required high antigen valency, as eOD trimers failed to show follicular localization, similar to eOD monomer (Fig. 2E, fig. S3G). Bare lumazine synthase nanoparticles lacking eOD also did not traffic to FDC networks (fig. S3H). Co-staining to identify germinal centers showed that both monomer and 60mer initiated GCs (Fig. 2F), but much higher levels of 60mer were localized in GCs, aligning with FDCs in the light zone (Fig. 2D, F). MD39–8mers and MD39-liposomes exhibited a similar pattern of concentration within germinal centers (fig. S3I–K).

Targeting to FDCs/germinal centers is not a generic property of nanoparticles in naïve animals, as many vaccine studies have shown particles of diverse sizes and material composition localizing in a manner suggesting exclusion rather than enrichment in B cell follicles (19–22). By contrast, immune complexes (ICs) have been reported to elicit a similar type of antigen delivery to FDCs (23–25). IC trafficking to FDCs is mediated by relay of complexes from subcapsular sinus macrophages to migrating B cells, which in turn transfer

antigen to FDCs, in a complement- and complement receptor-dependent manner (23–25). To determine if a related innate pathway is involved in the recognition of env nanoparticles, we immunized C3- and Cr1/2-deficient mice with eOD-60mer or MD39–8mer. As shown in Fig. 3A–B, both nanoparticles were strongly localized to the FDC network in wild-type mice at day 7, but only low levels of antigen were detected in $C3^{-/-}$ dLNs, with a diffuse distribution. Nanoparticle trafficking to FDCs was also abrogated in Cr1/2-deficient animals (Fig. 3C–D). Consistent with these findings, *in vitro* addition of normal serum to plate-immobilized eOD-60mer, but not eOD monomer or trimer, led to substantial deposition of C3 as detected by ELISA (Fig. 3E).

We next sought to define the mechanism of complement fixation by these nanoparticle immunogens. IgM from naïve animals did not bind eOD-60mer by ELISA (fig. S4), suggesting natural IgM is not involved. The lectin-mediated pathway activates complement in bacterial immunity; here, mannose-binding lectin (MBL) binds to glycosylated microbes and activates complement via MBL-associated serine proteases (26). MBL is a large macromolecular complex composed of multimers of trimeric lectin stalks, which achieve high avidity binding to pathogens through multivalent engagement with large patches of dense sugars (26–28). Structural studies have shown that the 3 carbohydrate binding domains (CBD) at the end of each stalk in the MBL multimer are arranged in a triangular configuration, separated by 4.5 nm (29); the distance between each stalk of MBL multimers is poorly defined but expected to be of similar order or larger (30). Each CBD recognizes mannose and other sugars with a very weak affinity of $K_D \sim 10^{-3}$ M, but stable binding to larger patches of glycans is thought to be achieved by the avidity effect of engaging multiple trimeric stalks of MBL multimers. These considerations suggest MBL will be unable to bind multiple stalks to an eOD monomer (diam. 7.5 nm) and may only be capable of engaging a few stalks on MD39 trimers (diam. 15 nm, fig. S5). In agreement with these arguments, in an ELISA-type assay murine and human MBL bound to immobilized eOD-60mer but exhibited only weak recognition of eOD-3mer and monomer (Fig. 4A). Biolayer interferometry measurements of eOD-60mer binding to immobilized MBL revealed an apparent affinity of ~4 pM, while binding by eOD monomer was essentially undetectable; similarly, MD39–8mer showed avid binding by MBL while binding to non-particulate MD39 was low (fig. S6A–B).

Following immunization of $MBL^{-/-}$ mice with eOD-60mer or MD39–8mer, dLNs contained low levels of antigen with no accumulation on the FDC network (Fig. 4B, fig. S7A–C). To evaluate if FDC localization was indeed immunogen-glycan dependent, we deglycosylated eOD-60mer with PNGase F, and confirmed by light scattering, TEM, and ELISA analysis that the enzyme-treated protein retained its self-assembled particle structure and presentation of the key CD4 binding site epitope (Fig. 4C–E, fig. S8). MBL bound at only low levels to deglycosylated eOD-60mer *in vitro* (fig. S6A), and deglycosylated particles exhibited low LN accumulation in WT mice with no FDC localization (Fig. 4F). These data imply that dense arrays of glycans trigger MBL-mediated innate immune recognition of nanoparticles. To assess the generality of this concept, we assessed trafficking of another highly glycosylated nanoparticle immunogen, influenza hemagluttinin (HA)-ferritin 8-mer particles (4), which were also targeted to the FDC network in wild type but not MBL KO mice (fig. S9A).

To obtain insight into how the composition and density of glycans regulates MBL recognition of nanoparticles, we characterized the glycan profiles of each of the immunogens. eOD-60mer was typically prepared in the presence of kifunensine, such that its glycans were almost completely oligomannose (fig. S10). By contrast, eOD monomer (typically prepared in 293F cells) contained predominantly complex-type glycans (fig. S10). To assess if this difference in glycan composition impacted *in vivo* antigen trafficking, we prepared eOD-60mer in 293F cells, which contained predominantly complex glycans mirroring the eOD monomer (fig. S10). These eOD-60mer nanoparticles trafficked to FDCs in a manner identical to the 60mer bearing only oligomannose glycans (fig. S9B), suggesting that small levels of oligomannose glycans are sufficient to trigger MBL-mediated trafficking to follicles. In support of this argument, MD39–8mers and HA-8mers exhibited a ~50/50 complex/oligomannose and predominantly complex glycan profile, respectively, but both nanoparticle immunogens showed similar FDC localization *in vivo*.

We then assessed the immunological impact of MBL recognition and FDC targeting. WT mice immunized with eOD-60mer showed a two-fold greater IgG response relative to deglycosylated 60mer (Fig. 4G). Further, responses to eOD-60mer were stronger in WT compared to MBL KO mice by several measures, with 53% greater T follicular helper cell responses, 43% greater germinal center B cell responses, and ~5-fold greater IgG titers across multiple antibody isotypes, irrespective of the adjuvant used (Fig. 4H–K and fig. S11A–B). IgG binding to plates coated with a low vs. high density of antigen was also proportionally weaker for sera from MBL KO animals compared to WT, suggesting a lower mean avidity of IgG elicited in MBL KO animals (fig. S11C). Eight weeks post immunization, WT mice also had approximately double the population of bone marrow-resident eOD-specific antibody secreting cells compared to MBL KO animals (Fig. 4L). Notably, MBL binding to eOD did not obscure recognition of the CD4 binding site (fig. S12), suggesting that innate recognition of env glycans would not inhibit generation of on-target antibody responses. Thus, despite preserving high multivalency for BCR triggering, nanoparticles lacking MBL-mediated FDC targeting elicit weaker humoral responses.

Finally, we assessed whether synthetic introduction of glycans could be used to engineer the delivery of nanoparticles to follicles, as a preliminary test of the utility of glycan engineering to alter the processing of nanoparticle vaccines *in vivo*. We expressed “bare” ferritin nanoparticles lacking any glycosylation; these particles showed low overall accumulation in LNs and no colocalization with FDCs following immunization in WT mice (Fig. 4M). By contrast, conjugation of a synthetic trimannose moiety to these nanoparticles led to pronounced accumulation on FDCs within 3 days of immunization (fig. S13A, Fig. 4M); this FDC localization was glycan density dependent because ferritin nanoparticles functionalized with a lower density of trimannose groups (~25 vs. ~96 trimannose groups per particle) did not localize to the FDC network (fig. S13B). To determine if glycan-mediated delivery to FDCs could be achieved with synthetic nanoparticles and to assess the effect of particle size, we functionalized monodisperse polystyrene nanoparticles with the same trimannose groups at high density (fig. S14A). PS nanoparticles 40 nm in diameter accumulated on FDCs (albeit with lower efficiency than the protein nanoparticles, possibly due to some level of aggregation *in vivo*), while 100 or 200 nm diam. particles were excluded from follicles (fig. S14B). Thus, synthetic introduction of even simple glycans by

chemical or genetic means may provide a means to direct arbitrary vaccine nanoparticles of appropriate size to the FDC network.

Collectively, these data suggest that glycosylated nanoparticles trigger MBL-mediated innate immune recognition, leading to rapid complement-dependent transport to FDCs and subsequent concentration in germinal centers *in vivo*. This targeted trafficking was associated with enhanced antibody responses, suggesting that tuning the glycosylation of immunogens may be a key design criterion for future nanoparticulate vaccines or immunomodulators, and providing an explanation for how FDC localization of immunogens can occur in the absence of pre-existing antibody. These findings are particularly interesting in the context of HIV vaccine development, where the dense "glycan shield" of envelope is usually viewed as a hurdle to elicitation of effective antibody responses.

Supplementary Material

Refer to Web version on PubMed Central for supplementary material.

Acknowledgments:

We thank the Koch Institute Swanson Biotechnology Center for technical support, specifically the Flow Cytometry, Microscopy, and Nanotechnology Materials Core Facilities. We also thank the Biophysical Instrumentation Facility for use of the Octet Bio-Layer Interferometry System.

Funding: This work was supported in part by the NIAID under Awards UM1AI100663 (to D.J.I, W.R.S., and M.C), AI104715 (to D.J.I.), and AI048240 (to D.J.I.), the Koch Institute Support (core) Grant P30-CA14051 from the National Cancer Institute, the Ragon Institute of MGH, MIT, and Harvard, and by the International AIDS Vaccine Initiative (IAVI) Neutralizing Antibody Consortium (NAC) and Center (to W.R.S. and M.C.); and through the Collaboration for AIDS Vaccine Discovery funding for the IAVI NAC Center (to W.R.S. and M.C.). IAVI's work is made possible by generous support from many donors, including the Bill & Melinda Gates Foundation, the Ministry of Foreign Affairs of Denmark, Irish Aid, the Ministry of Finance of Japan in partnership with The World Bank, the Ministry of Foreign Affairs of the Netherlands, the Norwegian Agency for Development Cooperation (NORAD), the UK Department for International Development (DFID), and the U.S. Agency for International Development (USAID). The full list of IAVI donors is available at www.iavi.org. The content is solely the responsibility of the authors and does not necessarily represent the official views of the National Institutes of Health. DJI is an investigator of the Howard Hughes Medical Institute.

References and Notes:

1. Bachmann MF, Jennings GT, Vaccine delivery: a matter of size, geometry, kinetics and molecular patterns. Nature Reviews Immunology 10, 787–796 (2010).
2. Naud PS et al., Sustained efficacy, immunogenicity, and safety of the HPV-16/18 AS04-adjuvanted vaccine: final analysis of a long-term follow-up study up to 9.4 years post-vaccination. Hum Vaccin Immunother 10, 2147–2162 (2014). [PubMed: 25424918]
3. Jackson Y, Chappuis F, Mezger N, Kanappa K, Loutan L, High immunogenicity of delayed third dose of hepatitis B vaccine in travellers. Vaccine 25, 3482–3484 (2007). [PubMed: 17306910]
4. Kanekiyo M et al., Self-assembling influenza nanoparticle vaccines elicit broadly neutralizing H1N1 antibodies. Nature 499, 102–106 (2013). [PubMed: 23698367]
5. Kanekiyo M et al., Rational Design of an Epstein-Barr Virus Vaccine Targeting the Receptor-Binding Site. Cell 162, 1090–1100 (2015). [PubMed: 26279189]
6. Jardine J et al., Rational HIV immunogen design to target specific germline B cell receptors. Science 340, 711–716 (2013). [PubMed: 23539181]
7. Abbott RK et al., Precursor Frequency and Affinity Determine B Cell Competitive Fitness in Germinal Centers, Tested with Germline-Targeting HIV Vaccine Immunogens. Immunity 48, 133–146 e136 (2018). [PubMed: 29287996]

8. Steichen JM et al., HIV Vaccine Design to Target Germline Precursors of Glycan-Dependent Broadly Neutralizing Antibodies. Immunity 45, 483–496 (2016). [PubMed: 27617678]
9. Ingale J et al., High-Density Array of Well-Ordered HIV-1 Spikes on Synthetic Liposomal Nanoparticles Efficiently Activate B Cells. Cell Rep 15, 1986–1999 (2016). [PubMed: 27210756]
10. Bale S et al., Covalent Linkage of HIV-1 Trimers to Synthetic Liposomes Elicits Improved B Cell and Antibody Responses. J Virol 91, (2017).
11. Martinez-Murillo P et al., Particulate Array of Well-Ordered HIV Clade C Env Trimers Elicits Neutralizing Antibodies that Display a Unique V2 Cap Approach. Immunity 46, 804–817 e807 (2017). [PubMed: 28514687]
12. Sliepen K et al., Presenting native-like HIV-1 envelope trimers on ferritin nanoparticles improves their immunogenicity. Retrovirology 12, 82(2015). [PubMed: 26410741]
13. Jardine JG et al., HIV-1 VACCINES. Priming a broadly neutralizing antibody response to HIV-1 using a germline-targeting immunogen. Science 349, 156–161 (2015). [PubMed: 26089355]
14. Jardine JG et al., HIV-1 broadly neutralizing antibody precursor B cells revealed by germline-targeting immunogen. Science 351, 1458–1463 (2016). [PubMed: 27013733]
15. Sok D et al., Priming HIV-1 broadly neutralizing antibody precursors in human Ig loci transgenic mice. Science 353, 1557–1560 (2016). [PubMed: 27608668]
16. Kulp DW et al., Structure-based design of native-like HIV-1 envelope trimers to silence non-neutralizing epitopes and eliminate CD4 binding. Nature communications 8, 1655(2017).
17. He L et al., Presenting native-like trimeric HIV-1 antigens with self-assembling nanoparticles. Nat Commun 7, 12041(2016). [PubMed: 27349934]
18. Park C, Arthos J, Cicala C, Kehrl JH, The HIV-1 envelope protein gp120 is captured and displayed for B cell recognition by SIGN-R1(+) lymph node macrophages. eLife 4, (2015).
19. Manolova V et al., Nanoparticles target distinct dendritic cell populations according to their size. Eur J Immunol 38, 1404–1413 (2008). [PubMed: 18389478]
20. Moon JJ et al., Enhancing humoral responses to a malaria antigen with nanoparticle vaccines that expand Tfh cells and promote germinal center induction. Proc Natl Acad Sci U S A 109, 1080–1085 (2012). [PubMed: 22247289]
21. Reddy ST, Rehor A, Schmoekel HG, Hubbell JA, Swartz MA, In vivo targeting of dendritic cells in lymph nodes with poly(propylene sulfide) nanoparticles. J Control Release 112, 26–34 (2006). [PubMed: 16529839]
22. Shukla S et al., Plant viral nanoparticles-based HER2 vaccine: Immune response influenced by differential transport, localization and cellular interactions of particulate carriers. Biomaterials 121, 15–27 (2017). [PubMed: 28063980]
23. Phan TG, Grigorova I, Okada T, Cyster JG, Subcapsular encounter and complement-dependent transport of immune complexes by lymph node B cells. Nat Immunol 8, 992–1000 (2007). [PubMed: 17660822]
24. Phan TG, Green JA, Gray EE, Xu Y, Cyster JG, Immune complex relay by subcapsular sinus macrophages and noncognate B cells drives antibody affinity maturation. Nat Immunol 10, 786–793 (2009). [PubMed: 19503106]
25. Carrasco YR, Batista FD, B cells acquire particulate antigen in a macrophage-rich area at the boundary between the follicle and the subcapsular sinus of the lymph node. Immunity 27, 160–171 (2007). [PubMed: 17658276]
26. Garred P et al., A journey through the lectin pathway of complement-MBL and beyond. Immunol Rev 274, 74–97 (2016). [PubMed: 27782323]
27. Ip WK, Takahashi K, Ezekowitz RA, Stuart LM, Mannose-binding lectin and innate immunity. Immunol Rev 230, 9–21 (2009). [PubMed: 19594626]
28. Howard M, Farrar CA, Sacks SH, Structural and functional diversity of collectins and ficolins and their relationship to disease. Semin Immunopathol 40, 75–85 (2018). [PubMed: 28894916]
29. Sheriff S, Chang CY, Ezekowitz RA, Human mannose-binding protein carbohydrate recognition domain trimerizes through a triple alpha-helical coiled-coil. Nat Struct Biol 1, 789–794 (1994). [PubMed: 7634089]

30. Turner MW, Mannose-binding lectin: the pluripotent molecule of the innate immune system. Immunol Today 17, 532–540 (1996). [PubMed: 8961631]

31. Wu X et al., Rational design of envelope identifies broadly neutralizing human monoclonal antibodies to HIV-1. Science 329, 856–861 (2010). [PubMed: 20616233]

32. Barouch DH et al., A human T-cell leukemia virus type 1 regulatory element enhances the immunogenicity of human immunodeficiency virus type 1 DNA vaccines in mice and nonhuman primates. J Virol 79, 8828–8834 (2005). [PubMed: 15994776]

33. Steichen JM et al., HIV Vaccine Design to Target Germline Precursors of Glycan-Dependent Broadly Neutralizing Antibodies. Immunity 45, 483–496 (2016). [PubMed: 27617678]

34. Lövgren-Bengtsson K, Morein B, in Methods in Molecular Medicine, Vaccine Adjuvants: Preparation Methods and Research Protocols, O'Hagan D, Ed. (Humana Press, Totowa, NJ, 2000), vol. 42, pp. 239–258.

35. Suan D et al., T follicular helper cells have distinct modes of migration and molecular signatures in naive and memory immune responses. Immunity 42, 704–718 (2015). [PubMed: 25840682]

36. Havenar-Daughton C et al., Cytokine-Independent Detection of Antigen-Specific Germinal Center T Follicular Helper Cells in Immunized Nonhuman Primates Using a Live Cell Activation-Induced Marker Technique. J Immunol, (2016).

37. Dan JM et al., A Cytokine-Independent Approach To Identify Antigen-Specific Human Germinal Center T Follicular Helper Cells and Rare Antigen-Specific CD4+ T Cells in Blood. J Immunol, (2016).

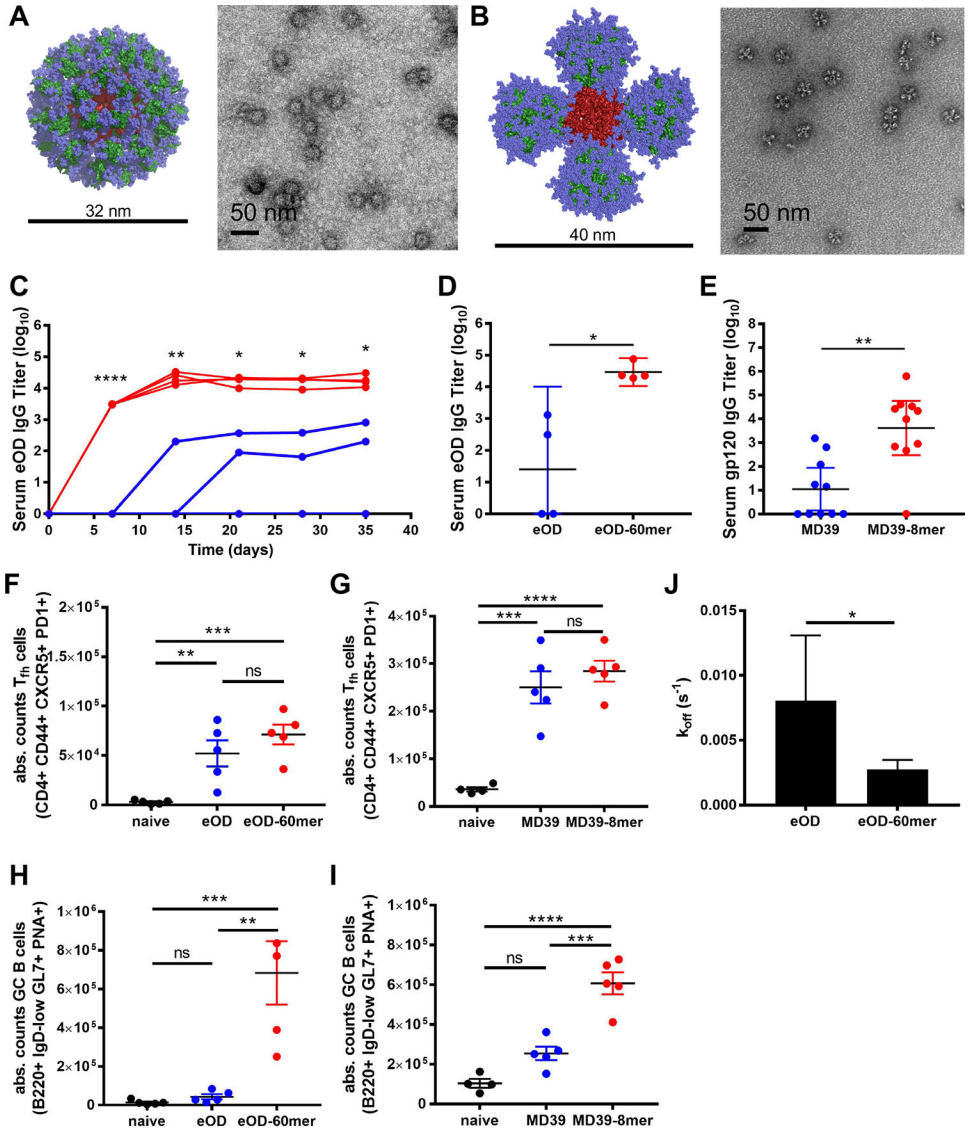

Fig. 1. Nanoparticle gp120 and env trimer immunogens elicit enhanced humoral immune responses.

(A, B) Model representations and TEM images of eOD-60mer (A) and MD39–8mer (B) nanoparticles. eOD or MD39 are shown in green, glycans shown in blue, and the lumazine synthase or ferritin core are in red. (C, D) Balb/c mice (n=4/group) were immunized with 2 μg eOD monomer (blue) or 3.7 μg eOD-60mer (red) containing the same moles of eOD and saponin adjuvant. Shown are serum eOD-specific IgG titers analyzed over time by ELISA (C) and titers 1 month post immunization (D). (E, F) Balb/c mice (n=5/group) were immunized with 1 μg MD39 or ~1.3 μg MD39–8mer containing the same moles of trimer and saponin adjuvant and boosted at 6 weeks; gp120-specific (E) IgG titers were analyzed 3 weeks post boost by ELISA. (F-I) Mice were immunized with eOD or MD39 as in panels C/E; antigen-specific Tfh cells (F, G) and GC B cells (H, I) in lymph nodes were enumerated by flow cytometry on day 7. (J) Dissociation rates of day 21 purified polyclonal IgG bound to immobilized eOD analyzed via bio-layer interferometry for mice immunized with eOD or

eOD-60mer. *p<0.05, **p<0.01, ***p<0.001, ****p<0.0001, determined using a Mann-Whitney test (serum titers), one-way ANOVA followed by Tukey's multiple comparisons test (GC/Tfh) or an unpaired *t* test.

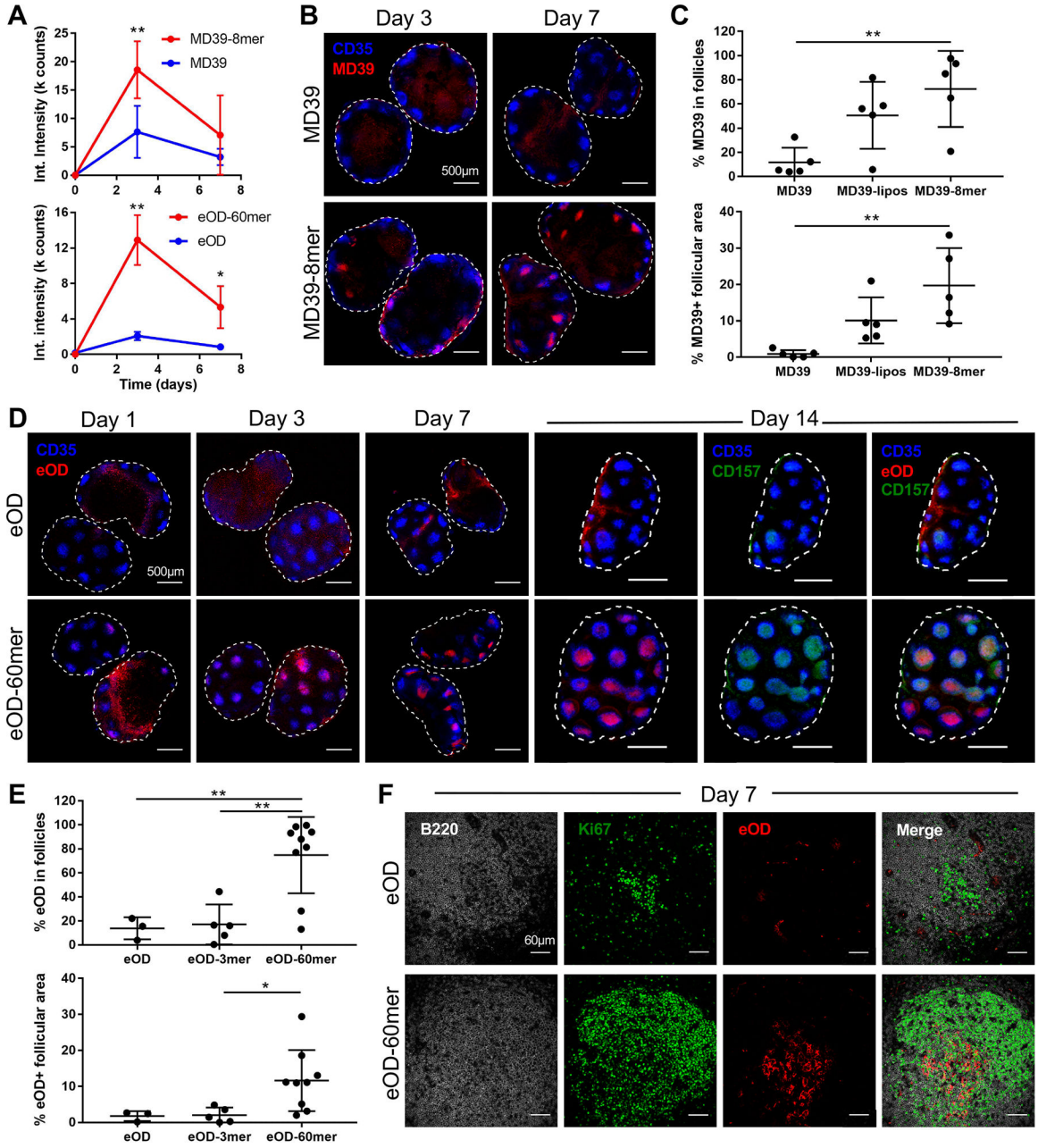

Fig. 2. Nanoparticle eOD and MD39 trimer immunogens are targeted to the FDC network and concentrate in germinal centers.

(A) Balb/c mice (*n*=4–5/group) were immunized with IR-dye-labeled MD39, MD39–8mer, eOD, or eOD-60mer and total fluorescence in dLNs was recorded over time. (B, C) Balb/c mice (*n*=5/group, 10 dLNs) were immunized with fluorescent MD39 or MD39–8mer (equivalent to 5 μg trimer in each group) and adjuvant. FDCs were labeled *in situ* with anti-CD35 antibody and excised dLNs were cleared and imaged by confocal microscopy (B) and colocalization of antigen with follicles was quantified (C). (D-F) Balb/c mice (*n*=5–9/group, 10–18 dLNs) were immunized with fluorescent eOD monomer or eOD-60mer (equivalent to 2 μg eOD in each group) and adjuvant. (D) FDCs or germinal centers were labeled *in situ*

with anti-CD35 or anti-CD157, respectively, and excised dLNs were cleared and imaged by confocal microscopy. In images from eOD-immunized mice, eOD brightness was increased to allow for visualization. (E) Colocalization of antigen with follicles was quantified. (F) dLNs were cut into 100 μm thick slices, stained with anti-B220 and anti-Ki67, and individual follicles were imaged by confocal microscopy. *$p<0.05$, **$p<0.01$, determined using a one-way ANOVA followed by Tukey's multiple comparisons test. LICOR analysis included comparisons to unimmunized LN controls at each time point.

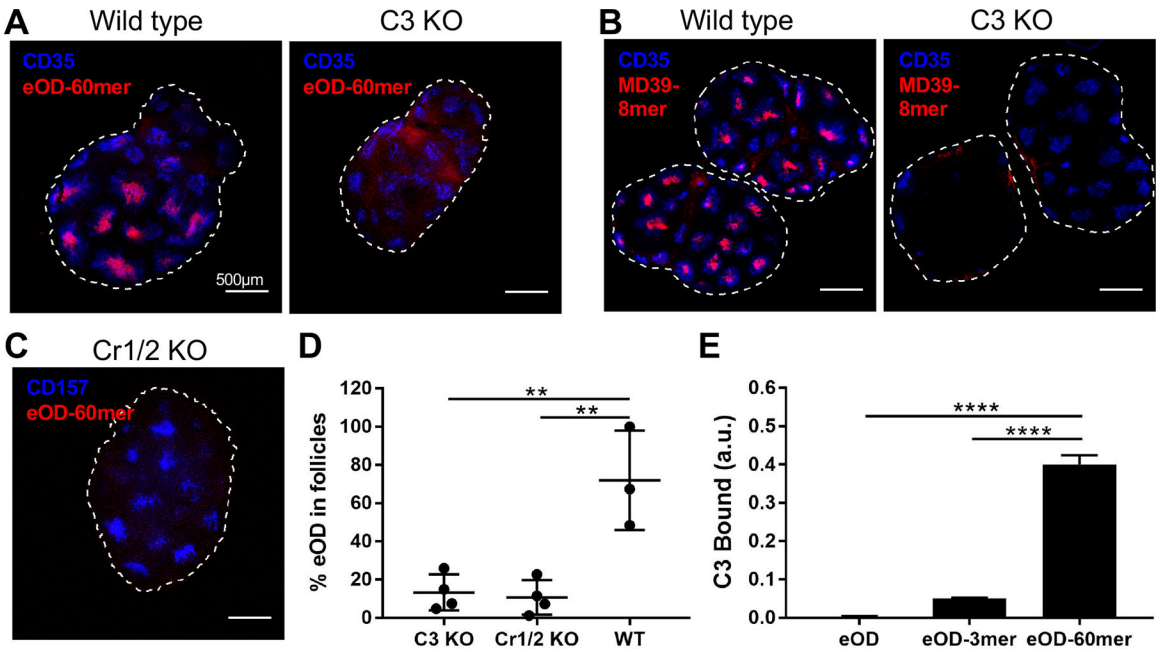

Fig. 3. Complement and complement receptor are required for follicular targeting of nanoparticle immunogens.

(A-D) Wild type C57BL/6, $C3^{-/-}$, or $Cr1/2^{-/-}$ mice (*n*=4/group, 8 dLNs) were immunized with 3.7 μg fluorescent eOD-60mer (equivalent to 2 μg eOD) or 6.4 μg MD39–8mer (equivalent to 5 μg trimer) and adjuvant. dLNs were recovered after 7 days, cleared, and imaged by confocal microscopy. Antigen localization was imaged in WT or knockout animal LNs for eOD-60mer (A, C) or MD39–8mer (B), and eOD localization in follicles in WT vs. knockout mice was quantified (D). (E) Wild-type mouse serum was added to plates coated with eOD monomer, eOD-3mer, or eOD-60mer, followed by detection of deposited C3 by ELISA. **p<0.01, ****p<0.0001, determined using a one-way ANOVA followed by Tukey's multiple comparisons test.

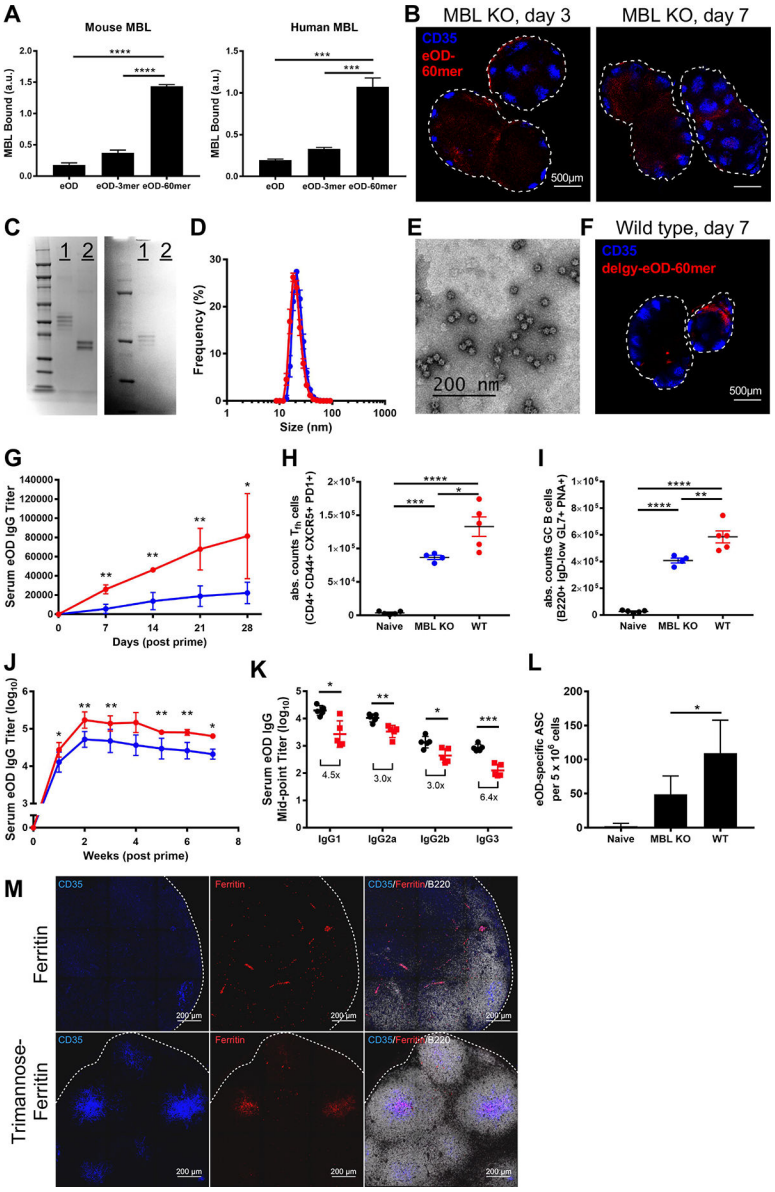

Fig. 4. Mannose-binding lectin-mediated innate recognition and follicular targeting amplifies humoral responses to env nanoparticle immunogens.

(A) Mouse (200 ng/ml) or human (7.5 μg/ml) MBL were added to plates coated with eOD monomer, eOD-3mer, or eOD-60mer, followed by detection of bound MBL by ELISA. (B) MBL$^{-/-}$ mice (n=3/group, 6 dLNs) were immunized with 3.7 μg fluorescent eOD-60mer (equivalent to 2 μg eOD) and adjuvant. Excised dLNs were cleared and imaged by confocal microscopy. eOD brightness was increased to allow for visualization. (C, D) Unmodified eOD-60mer (1) and eOD-60mer deglycosylated by PNGase F treatment (2) were analyzed via SDS-PAGE gel for changes in subunit size and glycan content (C, left: nonspecific protein stain, right: glycoprotein stain), dynamic light scattering (D, eOD-60mer, red; deglycosylated eOD-60mer, blue). (E) Cryo-TEM of deglycosylated eOD-60mer. (F) Mice (n=5/group, 10 dLNs) were immunized with 3.7 μg fluorescent deglycosylated eOD-60mer and adjuvant. Excised dLNs were cleared and imaged by confocal microscopy. (G) C57BL/6

mice (n=5/group) were immunized with 3.7 μg eOD-60mer (red) or deglycosylated eOD-60mer (blue) and adjuvant. Serum eOD-specific IgG titers were analyzed over time by ELISA. (H-L) C57BL/6 (red) or $MBL^{-/-}$ mice (blue; n=5/group) were immunized with 3.7 μg eOD-60mer and adjuvant. Total GC T_{fh} (H) and GC B cells (I) were analyzed at day 7; eOD-specific IgG titers were analyzed over time by ELISA (J); isotype specific mid-point titers were analyzed 1 month post immunization (K); and bone marrow eOD-specific ASCs were quantified by ELISPOT at 8 weeks post immunization (L). (M) C57BL/6 mice (n=3 animals/group) were immunized with 5 μg fluorescent bare ferritin nanoparticles lacking glycans, or ferritin particles conjugated with trimannose moieties (~96 trimannose groups/particle) together with adjuvant. LNs were excised 3 days later, sectioned, and imaged by confocal microscopy. *p<0.05, **p<0.01, ***p<0.001, ****p<0.0001, determined using either a one-way ANOVA followed by Tukey's multiple comparisons test or using a Mann-Whitney test (for serum titer analysis only).